PHYSICAL REVIEW D **92,** 051302(R) (2015)

# Reconstruction of energy spectra of neutrino beams independent of nuclear effects

X.-G. Lu,[1,*] D. Coplowe,[1] R. Shah,[1,2] G. Barr,[1] D. Wark,[1,2] and A. Weber[1,2]

[1]*Department of Physics, Oxford University, Oxford, Oxfordshire, United Kingdom*
[2]*STFC, Rutherford Appleton Laboratory, Harwell, Oxford, Oxfordshire, United Kingdom*

(Received 3 July 2015; published 21 September 2015)

We propose a new technique that enables an event-by-event selection of neutrino-hydrogen interactions in multinuclear targets and thereby allows application of hydrogen as targets in experiments with neutrino beams without involving cryogenics or high pressure hydrogen gas. This technique could significantly improve the reconstruction of the neutrino energy spectra. Since it allows a separation between hydrogen and the accompanying nuclei, this technique also enables us to measure nuclear effects in neutrino interactions directly.

DOI: 10.1103/PhysRevD.92.051302 PACS numbers: 13.15.+g, 14.20.Gk, 14.60.Lm, 29.27.Fh

The ability to measure the energy spectrum of a neutrino [1] beam has many physics implications [2,3]. The accuracy of the measurement depends on the spectral shape, the energy reconstruction, and the understanding of the cross sections of the processes by which the neutrino interactions are detected. The conventional measurement of the energy spectra of neutrino beams is via charged-current quasielastic scattering (CCQE) on nucleons: $\nu + \mathrm{n} \to l^- + \mathrm{p}$ and $\bar{\nu} + \mathrm{p} \to l^+ + \mathrm{n}$, where $\nu/\bar{\nu}$, n, p and $l^\mp$ stand for neutrino/antineutrino, neutron, proton, and the corresponding charged leptons, respectively. The neutrino energy can be calculated using the lepton momentum, assuming a static nucleon in the initial state [3,4]. With a nuclear target, the accuracy is limited by the binding energy and the Fermi motion (FM) of the nucleon, both subject to large fluctuations, and by other initial-state uncertainties. When the momentum of the final-state nucleon is measured, the neutrino energy can be reconstructed by summing all the final-state particle momenta. However, the kinematics of the final-state nucleon are altered by final-state interactions (FSIs) as the nucleon reinteracts with the cold nuclear medium before leaving the target nucleus. FSIs can be so strong that the nucleus is excited or even breaks up, emitting low momentum particles such as nucleons, photons, and pions, which are stopped near the vertex and not detected in tracking detectors, leading to greater bias in the reconstructed energy. Therefore, a third approach (not restricted to CCQE) is to sum the lepton energy and the visible energy of the hadronic system [2,5,6], which is limited by a reduced influence from nucleon initial-state uncertainties and by the systematics in measuring the energy of neutral particles. Among those initial-state uncertainties, multinucleon correlations [7–12] are under intense study. Such nuclear modifications make the calculation of the CCQE cross section difficult. Furthermore, in non-CCQE interactions such as resonance production, the final-state pions can rescatter, exchange charge, or be absorbed in the nuclear medium [13]. Such background events are often misidentified as CCQE due to the identical final-state particles and therefore introduce an ambiguity in the cross section definition. More details about neutrino-nucleus interactions can be found in Refs. [14,15] and references therein.

Hydrogen is the ideal target for reconstructing the neutrino energy because of the absence of these nuclear effects; however, a hydrogen target with high mass is technically impracticable. In this work, we propose a solution that uses a spatial symmetry in the final-state kinematics in charged-current (CC) resonance production to isolate hydrogen events in targets with a mixture of nuclei. This would allow the reconstruction of the beam energy spectrum only limited by the knowledge of the cross section on hydrogen, which is much better understood than those on nuclei.

Delta resonances $\Delta(1232)$ can be produced in CC interactions on hydrogen when the neutrino energy is above threshold (about 0.34 and 0.49 GeV for $\nu_\mathrm{e}$ and $\nu_\mu$, respectively). Consider a $\nu_\mathrm{e}$ or $\nu_\mu$ interaction on a proton $\nu + \mathrm{p} \to l^- + \Delta^{++}$, where the $\Delta^{++}$ decays to a proton and a positive pion, $\pi^+$. We define a double-transverse axis $\vec{z}_\mathrm{TT} \equiv \vec{p}_\nu \times \vec{p}_l / |\vec{p}_\nu \times \vec{p}_l|$, which is by construction perpendicular to both the neutrino and charged lepton momenta, $\vec{p}_\nu$ and $\vec{p}_l$. On projecting the proton and pion momenta, $\vec{p}_\mathrm{p}$ and $\vec{p}_\pi$, onto $\vec{z}_\mathrm{TT}$, $p^\mathrm{p}_\mathrm{TT} \equiv \vec{p}_\mathrm{p} \cdot \vec{z}_\mathrm{TT}$, $p^\pi_\mathrm{TT} \equiv \vec{p}_\pi \cdot \vec{z}_\mathrm{TT}$, one has the double-transverse momentum imbalance $\delta p_\mathrm{TT} \equiv p^\mathrm{p}_\mathrm{TT} + p^\pi_\mathrm{TT}$ (see Fig. 1 for a schematic illustration). In the absence of nuclear effects, as is expected for a hydrogen target, $\delta p_\mathrm{TT}$ is zero, whereas $\delta p_\mathrm{TT} \neq 0$ in the presence of FM and FSI in a nuclear target. This is independent of the neutrino energy and the resonance kinematics. The $\delta p_\mathrm{TT}$ for a nuclear target has the following properties: (1) It is distributed symmetrically around zero because the initial proton motion and the decay kinematics of the resonance are uncorrelated to $\vec{z}_\mathrm{TT}$ (except for uncommon cases such as polarized spatially asymmetric nuclear targets, or if the detection acceptance varies for different

*Xianguo.Lu@physics.ox.ac.uk

 

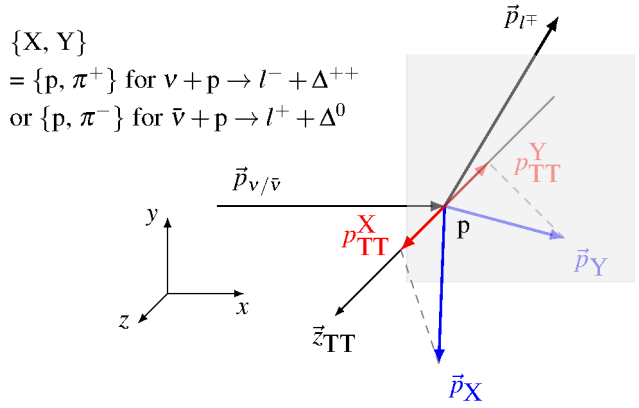


FIG. 1 (color online). Schematic illustration of the double-transverse kinematics. The incoming and outgoing particle momenta are represented by $\vec{p}_\nu$ and $\vec{p}_l$, $\vec{p}_\mathrm{p}$ and $\vec{p}_\pi$, respectively. The double-transverse momentum imbalance, $\delta p_\mathrm{TT}$, is given by $p^\mathrm{p}_\mathrm{TT} + p^\pi_\mathrm{TT}$ with respect to the axis $\vec{z}_\mathrm{TT}$ defined by $\vec{p}_\nu \times \vec{p}_l$.

final-state particles). (2) Since FM is isotropic, for a given initial proton momentum $p_\mathrm{p}$ (up to about 200 MeV/$c$ for carbon [16], for example), $\delta p_\mathrm{TT}$ is broadened from 0 to the same order of magnitude as $p_\mathrm{p}$. The randomness of FM further smears out $\delta p_\mathrm{TT}$. (3) The resonance and the decay products experience FSI. Such modification of the kinematics further adds to the broadening of the $\delta p_\mathrm{TT}$ distribution.

The difference between the $\delta p_\mathrm{TT}$ shapes for hydrogen and nuclear targets is dramatic (see Fig. 2). As can be seen in the figure, the shapes of the nuclear distributions predicted by NuWro [17] vary only slightly among nuclei heavier than deuteron. Therefore, for a multinuclear target with hydrogen, assuming perfect detector response, one expects a hydrogen signal at $\delta p_\mathrm{TT} = 0$ on top of a symmetric nuclear background that is about 200 MeV/$c$ wide. At the reconstruction level, the shape of the hydrogen peak, which is still symmetric, is solely determined by the

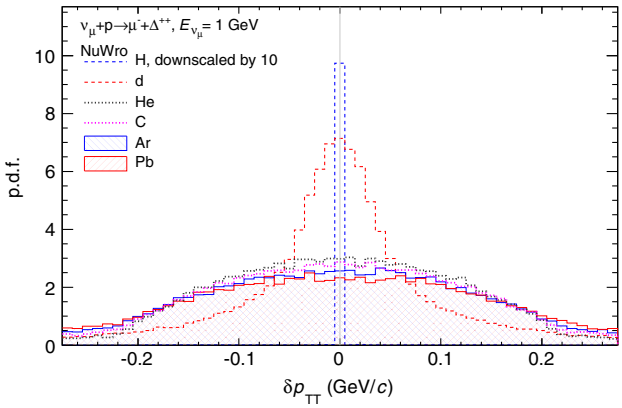


FIG. 2 (color online). Probability density function of the double-transverse kinematic imbalance $\delta p_\mathrm{TT}$ generated by NuWro [17] for hydrogen, deuteron, helium, carbon, argon, and lead targets with neutrino energy of 1 GeV. The width of the hydrogen distribution is due to the finite bin width.

detector response. The nuclear background contamination under the hydrogen peak depends on the background shape and the resonance production cross section ratio between the nucleus and hydrogen, which equals roughly the atomic number of the nucleus modulo nuclear effects. Improving the detector resolution [18] will lead to a strong signal enhancement and eventually an event-by-event selection of hydrogen interactions. Once the hydrogen interactions are selected, the neutrino energy can be reconstructed by summing the final-state energy [19]. The energy reconstruction quality is solely determined by detector response and not limited by nuclear effects.

The advantage of $\delta p_\mathrm{TT}$ is clear when compared to other characteristic variables in the interaction such as the invariant mass of $\Delta(1232)$ and the total transverse momentum. The former has an irreducible Breit-Wigner width of about 117 MeV/$c^2$ [20] and therefore has no sensitivity to reject nuclear background; the latter, which is intrinsically also zero for a hydrogen target, is asymmetric after reconstruction and in general has a long tail resembling the Landau distribution [21] due to detector effects.

For the antineutrino interaction on a proton $\bar{\nu} + \mathrm{p} \to l^+ + \Delta^0$, where $\Delta^0$ decays to $\mathrm{p} + \pi^-$, the previous definition and discussions directly apply. This similarity enables highly consistent measurements of neutrino and antineutrino energy spectra.

Given limited detector resolution, it is important to minimize background that has nonzero $\delta p_\mathrm{TT}$. Because FSI can lead to soft nuclear emission, measuring the vertex energy [22,23] allows tagging and rejecting interactions on other nuclei. And since pion FSI can modify the final states, the hydrogen signal purity could be enhanced by choosing target materials whose nuclear part has a large pion FSI cross section. Nonexclusive background such as multiple pion production can be rejected by vetoing electromagnetic processes and neutral particles [24].

For existing experiments, given a well-understood detector response, it may be feasible to perform a combined fit to the center region of the $\delta p_\mathrm{TT}$ distribution for a mixed target, where the hydrogen shape is fixed and the background modeling follows the general properties described above. If the signal width is at the subhundred MeV level, the fit may not be sensitive to the detail of the complicated nuclear tails. The cross section of the resonance production on hydrogen, which is independent of nuclear effects, can be obtained from the signal part. The yield ratio between the hydrogen signal and the remaining contribution from the other target nuclei is a precise measurement of the associated nuclear effects with cancellation of detection acceptance and efficiencies for both targets. Such measurement of the resonance production on hydrogen and nuclei should largely improve the understanding of the production mechanism and its modification by the nuclear medium.

More challenging background processes are those with intrinsic zero $\delta p_\mathrm{TT}$. One type of such background is the

exclusive processes that have identical final states as the signal, such as higher mass resonances and nonresonant production [25]. Those processes do not affect the neutrino energy reconstruction, but make it difficult to define the interaction cross section which is needed to determine the beam energy spectrum. To distinguish among underlying processes, the detailed interaction kinematics could be used, such as the invariant mass of the hadronic system $W$ and the squared four-momentum exchange to the proton $t$. This is feasible thanks to the essential features—being exclusive and nuclear effect independent—that make the neutrino energy reconstruction precise. Because the cross sections have different dependence on $W$ and $t$, efficient separation should be possible. Since the relevant final-state kinematics do not depend on the identity of the intermediate state, alternatively one could extend the definition of the production channel to include all contributions that have exclusive $p\pi^+$ final states and calculate the corresponding cross section [26,27]. Another type of background is the $\nu_\mu$ ($\bar{\nu}_\mu$) contamination in the $\bar{\nu}_\mu$ ($\nu_\mu$) CC interaction. Such "wrong sign" background occurs more often in an antineutrino beam created in a proton accelerator. Because of the similar particle identification (PID) signals for the muon and pion, the $\mu^- + \pi^+ + p$ final states from the $\nu_\mu$ background might be misidentified in the event selection as $\pi^- + \mu^+ + p$ from $\bar{\nu}_\mu$, and vice versa. For a large enough detection volume, the properties of stopped pions can be used to enhance the pion identification. In addition to measuring trajectory "kinks" [28] and the Michel electrons [29], negative pions that are stopped and absorbed by nuclei give rise to soft nuclear emission that can be measured by calorimetry [30]. The lepton, $\pi^+$, and $\pi^-$ signatures are different and serve as an important tool not only for $l/\pi$ separation, but also for rejecting wrong sign contamination. In addition, variables like $W$, which is calculated from the true $p\mu$ system due to wrong PID, can provide background rejection power due to the unphysical kinematic combination [31].

In this work, MC simulation of the T2K ND280 detector [32] is used to demonstrate the measurement of CC resonance production in neutrino-hydrogen interactions, $\nu_\mu + H \to \mu^- + \Delta^{++}$. Neutrino interactions in ND280 are simulated using the Neut event generator [33]. The event reconstruction uses the first fine-grained detector (FGD [34]) as a plastic scintillator (polystyrene) interaction target and the neighboring gaseous time projection chamber (TPC [35]) downstream to measure the momenta and specific energy loss ($dE/dx$) of the final-state particles. There are about 300 true $\Delta^{++}$ events on hydrogen in the neutrino energy range $0.5 < E_{\nu_\mu} < 5$ GeV in the reconstructed sample.

The distribution of the reconstructed double-transverse kinematic imbalance $\delta p_{TT}$ in the ND280 acceptance (detection efficiencies apply) is shown in Fig. 3. Because of the absence of nuclear effects, for hydrogen the resolution is

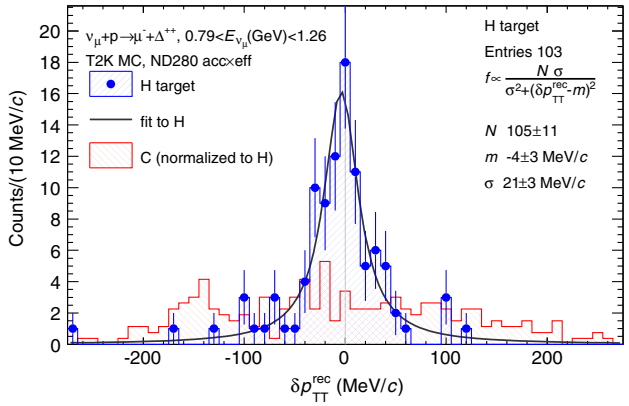


FIG. 3 (color online). Distributions of the reconstructed $\delta p_{TT}$ in the ND280 acceptance (detection efficiencies apply) simulated for hydrogen and carbon target nuclei in the neutrino energy range 0.79–1.26 GeV. Vertical bars are MC statistical errors. The hydrogen signal is fit to a Cauchy distribution. The carbon distribution is area normalized to the hydrogen.

determined by the detector response, which can be described in the simulation by a Cauchy function $1/N \cdot dN/d\delta p_{TT} = 1/\pi \cdot \sigma/[\sigma^2 + (\delta p_{TT} - m)^2]$ with the event count $N$, mean $m$, and width $\sigma$. The resolution is shown to be significantly smaller than the nuclear broadening in the carbon target nuclei. The nuclear rejection factor defined as the efficiency ratio between hydrogen and carbon is about 3.7 (2.3) in the 1 (3) $\sigma$ interval. The reconstruction performance of $\delta p_{TT}$ as a function of the neutrino energy is shown in Fig. 4. It indicates a better hydrogen selection at lower energy.

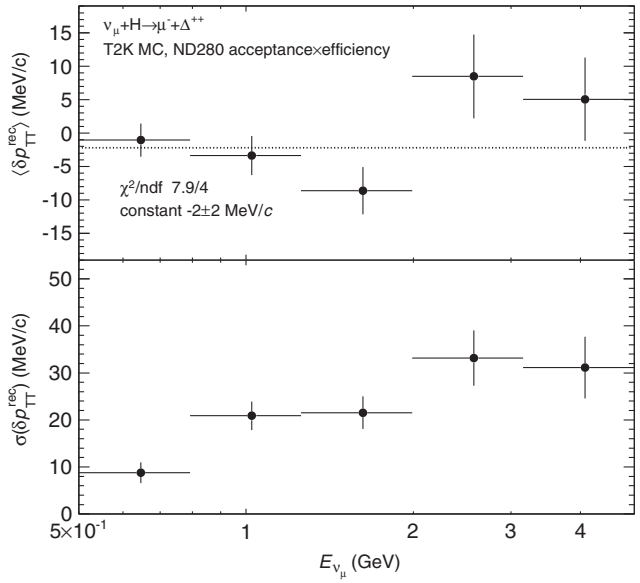


FIG. 4. The Cauchy mean (upper) and width (lower) of the reconstructed $\delta p_{TT}$ as a function of the neutrino energy. Vertical bars are MC statistical errors, while horizontal error bars stand for the bin span of the neutrino energy. A fit of a constant is applied to the mean values.

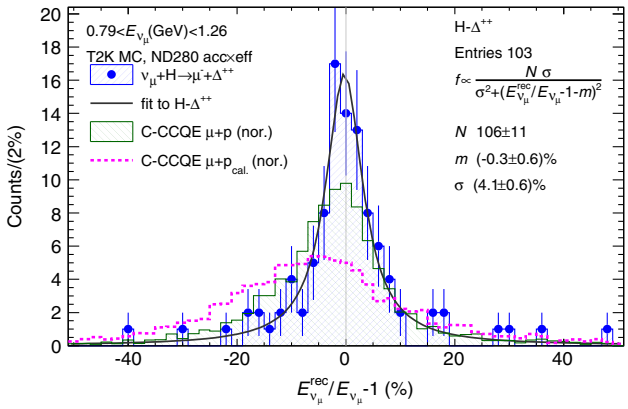


FIG. 5 (color online). Deviation of the reconstructed neutrino energy from the true value. Reconstruction with the CC resonance production on hydrogen targets is compared to the ones using CCQE on carbon: one summing both muon and proton reconstructed kinematics ("$\mu + \mathrm{p}$"), the other using the muon to calculate the proton momentum assuming a static initial neutron ("$\mu + \mathrm{p_{cal}}$") [4]. The carbon distributions are area normalized to the hydrogen.

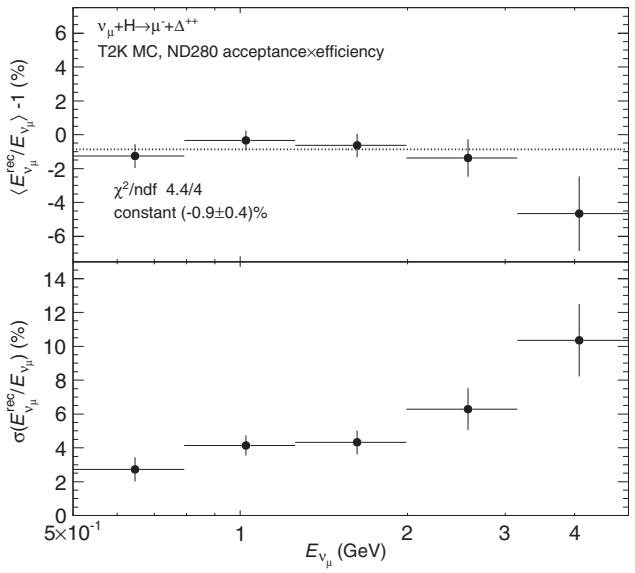


FIG. 6. Neutrino energy scale (upper) and reconstruction resolution (lower) via CC resonance production on hydrogen.

From the MC true hydrogen-resonance events in the reconstructed sample, the neutrino energy $E_{\nu_\mu}$ is calculated directly using the kinematics of all final-state particles. The uncertainty in an example $E_{\nu_\mu}$ bin is shown in Fig. 5. Like $\delta p_{\mathrm{TT}}$, it is determined by pure detector resolution due to the free and static proton target and can be described by a Cauchy function. As a comparison, the neutrino energy in the same range is reconstructed with all final-state kinematics from CCQE interactions on carbon assuming static neutron targets. This simple reconstruction suffers from nuclear effects in addition to the detector resolution and is biased by about $-2\%$ with a large spread. In addition, the neutrino energy distribution reconstructed only with the muon kinematics [4,36] shows worse performance. The comparison between both CCQE methods indicates that, for the relatively weak FSI predicted in the current model, an independent measurement of the proton kinematics helps improve the $E_{\nu_\mu}$ resolution even in the presence of FSI. The simulated $E_{\nu_\mu}$ detector response (the Cauchy mean and width) is further shown as a function of the true energy in Fig. 6. The energy scale is seen to be constant with a bias of about $-1\%$, and the resolution slowly increases from about 3% to 10% in the 0.5–5 GeV region. The worsening of resolution at high energy is general for a tracker measurement, in contrast to calorimetry [2,5,6].

Given the fact that ND280 was optimized to measure CCQE interactions and designed to achieve a performance that was to be limited by the nucleon initial-state uncertainties in the nuclear target [34,35], alternative optimization and state-of-the-art technology may allow better performance. Since the CC resonance production cross section rises to a maximum at a neutrino energy greater than about 3 GeV [20], the high energy neutrinos produced in the NuMI [37] and LBNF [2] beam lines are optimal to realize the proposed method. It would be challenging, yet very attractive, to combine the proposed use of hydrogen targets and the liquid argon TPC projects [2,38–41] which are to realize superb tracking and calorimetry performance on a massive scale. Finally, it would be interesting to demonstrate the method with antineutrino beams as well as for $\nu_\mathrm{e}/\bar{\nu}_\mathrm{e}$ interactions in oscillation appearance and investigate the impact on the physics programs in future experiments, considering also the advantage of the identical target, interaction kinematics and phase space in the proposed channels $\nu/\bar{\nu} + \mathrm{p} \to l^{\mp} + \Delta \to l^{\mp} + \mathrm{p} + \pi^{\pm}$, in comparison to the conventional CCQE interactions.

## ACKNOWLEDGMENTS

The authors express their gratitude to the T2K experiment for the use of the full MC production and the excellent analysis software in this study, and to T. Dealtry, K. Duffy, R. Guenette, A. Jacob, K. McFarland, V. Paolone, L. Pickering, F. Sanchez, H. Tanaka, Y. Uchida, M. Wascko, C. Wilkinson, M. Yokoyama and M. Zito for helpful discussions. We are grateful to R. Guenette and Y. Uchida for useful suggestions on improving the manuscript. This work is supported by the UK Science and Technology Facilities Council.

[1] In this paper, unless otherwise specified, *neutrino* refers to both *neutrino* and *antineutrino*.

[2] C. Adams *et al.* (LBNE Collaboration), Reports No. BNL-101354-2013-JA, No. BNL-101354-2014-JA, No. FERMILAB-PUB-14-022, and No. LA-UR-14-20881, 2013.

[3] K. Abe *et al.* (Hyper-Kamiokande Proto-Collaboration), Physics potential of a long-baseline neutrino oscillation experiment using a J-PARC neutrino beam and Hyper-Kamiokande, Prog. Theor. Exp. Phys. **2015**, 53C02 (2015).

[4] K. Abe *et al.* (T2K Collaboration), Observation of Electron Neutrino Appearance in a Muon Neutrino Beam, Phys. Rev. Lett. **112**, 061802 (2014).

[5] D. S. Ayres *et al.* (NOvA Collaboration), NOvA: proposal to build a 30 kiloton off-axis detector to study $\nu_\mu \to \nu_e$ oscillations in the NuMI beamline, arXiv:hep-ex/0503053.

[6] D. G. Michael *et al.* (MINOS Collaboration), Observation of Muon Neutrino Disappearance with the MINOS Detectors and the NuMI Neutrino Beam, Phys. Rev. Lett. **97**, 191801 (2006).

[7] K. S. Egiyan *et al.* (CLAS Collaboration), Measurement of 2- and 3-Nucleon Short Range Correlation Probabilities in Nuclei, Phys. Rev. Lett. **96**, 082501 (2006).

[8] R. Shneor *et al.* (Jefferson Lab Hall A Collaboration), Investigation of Proton-Proton Short-Range Correlations via the $^{12}C(e, e'pp)$ Reaction, Phys. Rev. Lett. **99**, 072501 (2007).

[9] A. A. Aguilar-Arevalo *et al.* (MiniBooNE Collaboration), First measurement of the muon neutrino charged current quasielastic double differential cross section, Phys. Rev. D **81**, 092005 (2010).

[10] A. A. Aguilar-Arevalo *et al.* (MiniBooNE Collaboration), First measurement of the muon antineutrino double-differential charged-current quasielastic cross section, Phys. Rev. D **88**, 032001 (2013).

[11] M. Martini, M. Ericson, G. Chanfray, and J. Marteau, Neutrino and antineutrino quasielastic interactions with nuclei, Phys. Rev. C **81**, 045502 (2010).

[12] J. Nieves, I. Ruiz Simo, and M. J. Vicente Vacas, The nucleon axial mass and the MiniBooNE quasielastic neutrino-nucleus scattering problem, Phys. Lett. B **707**, 72 (2012).

[13] D. Ashery and J. P. Schiffer, Pion absorption in nuclei, Annu. Rev. Nucl. Part. Sci. **36**, 207 (1986).

[14] H. Gallagher, G. Garvey, and G. P. Zeller, Neutrino-nucleus interactions, Annu. Rev. Nucl. Part. Sci. **61**, 355 (2011).

[15] J. A. Formaggio and G. P. Zeller, From eV to EeV: neutrino cross sections across energy scales, Rev. Mod. Phys. **84**, 1307 (2012).

[16] B. Povh, K. Rith, C. Scholz, and F. Zersche, *Particles and Nuclei: An Introduction to the Physical Concepts* (Springer, Berlin, 2009), p. 428.

[17] T. Golan, C. Juszczak, and J. T. Sobczyk, Final-state interactions effects in neutrino-nucleus interactions, Phys. Rev. C **86**, 015505 (2012).

[18] Concerning the resolution, there is some flexibility to optimize the signal selection: any of the final-state momentum directions can be used to construct $\vec{z}_{\mathrm{TT}}$ and only the momenta of the other two particles are required for reconstructing $\delta p_{\mathrm{TT}}$.

[19] Depending on the tracking, calorimetry and particle identification performance of a detector, alternative calculation of the neutrino energy by summing the longitudinal components of the final-state momenta could be considered.

[20] K. A. Olive *et al.* (Particle Data Group Collaboration), Review of particle physics, Chin. Phys. C **38**, 090001 (2014).

[21] L. D. Landau, On the energy loss of fast particles by ionization, J. Phys. (USSR) **8**, 201 (1944); See also *Collected Papers of L. D. Landau*, edited by D. Ter Haar (Gordon and Breach Science, New York, 1965), p. 417.

[22] L. Fields *et al.* (MINERvA Collaboration), Measurement of Muon Antineutrino Quasielastic Scattering on a Hydrocarbon Target at E3.5 GeV, Phys. Rev. Lett. **111**, 022501 (2013).

[23] G. A. Fiorentini *et al.* (MINERvA Collaboration), Measurement of Muon Neutrino Quasielastic Scattering on a Hydrocarbon Target at E3.5 GeV, Phys. Rev. Lett. **111**, 022502 (2013).

[24] D. Allan *et al.* (T2K UK Collaboration), The electromagnetic calorimeter for the T2K near detector ND280, J. Instrum. **8**, P10019 (2013).

[25] In coherent pion production on hydrogen, the slowly recoiling proton usually escapes detection. Therefore, coherent pion production in general is not a background process.

[26] S. L. Adler, Photoproduction, electroproduction, and weak single pion production in the (3,3) resonance region, Ann. Phys. (N.Y.) **50**, 189 (1968).

[27] D. Rein and L. M. Sehgal, Neutrino excitation of baryon resonances and single pion production, Ann. Phys. (N.Y.) **133**, 79 (1981).

[28] B. B. Abelev *et al.* (ALICE Collaboration), Performance of the ALICE Experiment at the CERN LHC, Int. J. Mod. Phys. A **29**, 1430044 (2014).

[29] A. A. Aguilar-Arevalo *et al.* (MiniBooNE Collaboration), Measurement of the neutrino component of an antineutrino beam observed by a nonmagnetized detector, Phys. Rev. D **84**, 072005 (2011).

[30] A. Marin, J. Diaz, R. Averbeck, A. Doppenschmidt, S. Hlavac, R. Holzmann, F. Lefevre, A. Schubert *et al.*, Detection of charged pions and protons in the segmented electromagnetic calorimeter TAPS, Nucl. Instrum. Methods Phys. Res., Sect. A **417**, 137 (1998).

[31] J. Campbell, G. Charlton, Y. Cho, M. Derrick, R. Engelmann, J. Fetkovich, L. Hyman, K. Jaeger *et al.*, Study of the Reaction $\nu p \to \mu^- \pi^+ p$, Phys. Rev. Lett. **30**, 335 (1973).

[32] K. Abe *et al.* (T2K Collaboration), The T2K experiment, Nucl. Instrum. Methods Phys. Res., Sect. A **659**, 106 (2011).

[33] Y. Hayato, Neut, Nucl. Phys. B Proc. Suppl. **112**, 171 (2002).

[34] P. A. Amaudruz *et al.* (T2K ND280 FGD Collaboration), The T2K fine-grained detectors, Nucl. Instrum. Methods Phys. Res., Sect. A **696**, 1 (2012).

[35] N. Abgrall *et al.* (T2K ND280 TPC Collaboration), Time projection chambers for the T2K near detectors,

Nucl. Instrum. Methods Phys. Res., Sect. A **637**, 25 (2011).

[36] In water Cherenkov detectors, the final-state protons are mostly below detection threshold. In such cases the neutrino energy can only be estimated using the muon kinematics.

[37] K. Anderson, B. Bernstein, D. Boehnlein, K. R. Bourkland, S. Childress, N. Grossman, J. Hylen, C. James *et al.*, Report No. FERMILAB-DESIGN-1998-01.

[38] H. Chen *et al.* (MicroBooNE Collaboration), Report No. FERMILAB-PROPOSAL-0974.

[39] C. Anderson, M. Antonello, B. Baller, T. Bolton, C. Bromberg, F. Cavanna, E. Church, D. Edmunds *et al.*, The ArgoNeuT detector in the NuMI low-energy beam line at Fermilab, J. Instrum. **7**, P10019 (2012).

[40] C. Adams *et al.* (LArTPC Collaboration), LAr1-ND: testing neutrino anomalies with multiple LArTPC detectors at Fermilab, arXiv:1309.7987.

[41] M. Antonello, B. Baibussinov, V. Bellini, H. Bilokon, F. Boffelli, M. Bonesini, E. Calligarich, S. Centro *et al.*, ICARUS at FNAL, arXiv:1312.7252.